Journal of Machine Engineering, 2026, Vol. 26,
ISSN 1895-7595 (Print) ISSN 2391-8071 (Online)

Received*: 16 November 2025* / Accepted: *10 March 2026* / Published online: *16 April 2026*

on-board charger (OBC),
LCL Filter,
active damping,
vehicle-to-grid (V2G)

Anas DIOURI[1*], Mohamed KHAFALLAH[1],
Abdelilah HASSOUNE[1,2], Mohammed Amine MESKINI[1]

COMPARATIVE EVALUATION OF LCL FILTER DAMPING STRATEGIES FOR BIDIRECTIONAL EV ON-BOARD CHARGERS UNDER G2V AND V2G OPERATION

This paper presents a comparative evaluation of passive and active damping techniques for LCL filters in bidirectional onboard chargers (OBCs) used in electric vehicle (EV) applications. The investigated system consists of an LCL-filtered Active Front-End (AFE) converter, an 800 V DC-link, and a bidirectional non-isolated DC/DC stage interfacing with a 360 V lithium-ion battery, enabling both Grid-to-Vehicle (G2V) and Vehicle-to-Grid (V2G) operation. The LCL filter is designed to satisfy harmonic attenuation and reactive power constraints, with the resonance frequency targeted near 1.2 kHz. Three passive damping approaches—series, parallel, and R–C branch damping—are analysed and compared with active damping based on capacitor-current feedback. Transfer-function modelling and Bode-plot analysis are used to examine resonance characteristics, while time-domain perturbation tests in MATLAB/Simulink evaluate grid-current quality under both power-flow directions. The results show that passive damping effectively suppresses resonance but may introduce additional losses or reactive power variation. Active damping provides the best THD performance and maintains stable operation under bidirectional conditions, although at the cost of increased control complexity. The study highlights the trade-offs between damping effectiveness, implementation complexity, and grid-compliance constraints, providing practical guidance for the design of robust LCL-filtered EV onboard chargers.

1. INTRODUCTION

The accelerated deployment of Electric Vehicles (EVs) has led to significant interest in high-performance, grid-compliant onboard chargers (OBCs) that enable both unidirectional and bidirectional power flows [1–2]. As EV penetration increases, the opportunity for V2G systems to enhance grid flexibility, provide ancillary services, and support renewable integration has become a key research priority [3–4]. Within this context, the onboard charger plays a pivotal role in ensuring safe, efficient, and compliant energy exchange between the vehicle and the grid [5–7].

[1] Laboratory of Energy & Electrical Systems (LESE), Superior National School of Electricity and Mechanical (ENSEM), Hassan II University, Casablanca, Morocco
[2] ENSA Beni Mellal, Sultan Moulay Slimane University, Beni Mellal, Morocco
[*] E-mail: anas.diouri-etu@etu.univh2c.ma
https://doi.org/10.36897/jme/219078

To meet power quality standards such as IEEE 1547 and IEC 61000-3-2, grid-connected onboard chargers (OBCs) typically require front-end power factor correction (PFC) stage [8-9]. The equivalent circuit representations of the L, LC, and LCL filters are shown in Fig 1. The LCL filter is widely preferred in these applications due to its superior attenuation of high-frequency switching harmonics compared to traditional L or LC filters [8-9]. However, LCL filters introduce a resonant peak in the frequency domain that can compromise stability and degrade control performance, especially in weak grids or during bidirectional operation [9].

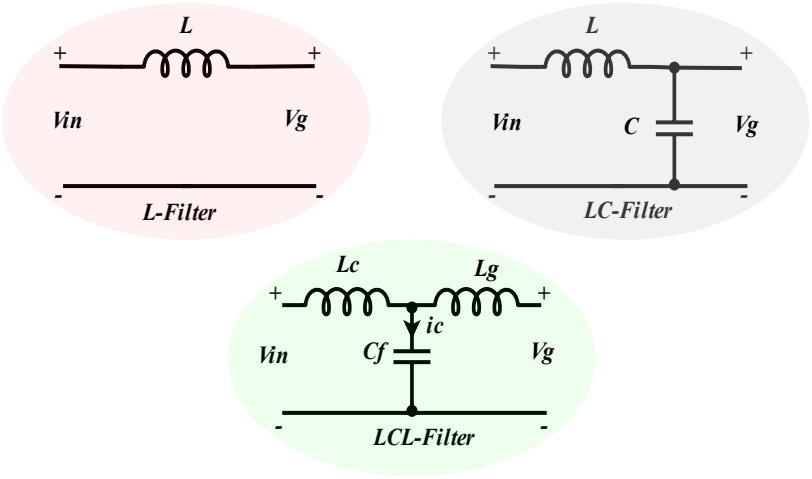

Fig. 1. Equivalent circuit representations of L, LC, and LCL filters used for grid-connected converters. Lc: inverter-side inductor; Lg: grid-side inductor; Cf: filter capacitor

This has motivated extensive research into damping techniques, which aim to suppress the resonant peak while preserving filter performance and minimizing energy losses [10-12]. Conventional passive damping methods, such as series or parallel resistors, are straightforward to implement but inherently dissipate power and can affect reactive power flow [11]. Advanced configurations like the R-C damping branch offer improved control over resonance but must be carefully designed to remain within reactive power constraints [12]. On the other hand, active damping techniques—such as capacitor current feedback and virtual impedance—achieve resonance suppression through control modifications, avoiding resistive losses but introducing sensitivity to digital implementation delays and grid parameter variations [13-17].

Recent studies have extensively analyzed damping methods, often focusing on isolated scenarios or under idealized unidirectional operation assumptions [18]. This paper aims to bridge this gap by presenting a unified comparative study of passive and active damping strategies applied to LCL filters within a realistic, bidirectional 10 kW onboard charger (OBC) environment. The proposed setup encompasses both Grid-to-Vehicle (G2V) and Vehicle-to-Grid (V2G) modes, evaluating the damping methods through Bode analysis, resonance perturbation tests, and harmonic distortion metrics. Building upon and extending earlier research [6-7], this study integrates practical design insights, filter analysis, and harmonized MATLAB/Simulink evaluations, targeting real-world compliance and stability considerations.

The rest of this paper is organized as follows. Section 2 presents the mathematical modelling and design procedure of the LCL filter used in the grid interface. Section 3 examines several passive damping approaches, including series resistor, parallel resistor, and R–C branch configurations. Section 4 then introduces the active damping strategy based on capacitor-current feedback and its integration within the control structure. Section 5 provides a comparative assessment of passive and active damping techniques from a practical implementation perspective. Section 6 reports the simulation results obtained under both Grid-to-Vehicle (G2V) and Vehicle-to-Grid (V2G) operating conditions. Finally, Section 7 summarizes the main findings and discusses possible directions for future work.

2. LCL FILTER DESIGN

This chapter focuses on the practical design methodology of an LCL filter for a bidirectional grid-connected converter. The goal is to maintain control stability and minimizing reactive power injection.

2.1. BASE PARAMETER COMPUTATION

To normalize the filter design, base values of voltage, current, and impedance are defined from the rated apparent power and grid voltage [8–9].

$$Z_{base} = \frac{V_{ph}^2}{S_{rated}} \tag{1}$$

$$C_{base} = \frac{1}{\omega_{grid} Z_{base}} \tag{2}$$

where: $V_{ph} = \frac{V_{LL}}{\sqrt{3}}$, and $\omega_{grid} = 2\pi f_{grid}$

2.2. FILTER CAPAC ITOR DESIGN

The capacitor C_f provides a low-impedance path for high-frequency harmonics and improves grid current quality. Its reactive-power contribution must remain below 5% of the converter's apparent power to comply with grid codes [9–10].

$$C_f = \alpha \cdot C_{base}, \alpha \in [0.02,0.05] \tag{3}$$

The value of C_f is obtained from (3) to satisfy this constraint.

2.3. FILTER INVERTER-SIDE INDUCTOR DESIGN

To limit the current ripple at the switching frequency the inverter-side inductance is determined as [8–9]:

$$L_c = \frac{V_{dc}}{8 \cdot f_{sw} \cdot \Delta I} \tag{4}$$

Where Vdc is the DC-link voltage, and ΔI is the peak-to-peak ripple current (usually 20% of rated).

2.4. FILTER GRID-SIDE INDUCTOR DESIGN

A balanced design often used to simplify bidirectional control implementation [8–9]:

$$L_g = L_c \tag{5}$$

Though *Lg>Lc* may be chosen in EMI-sensitive or weak-grid cases [9].

2.5. RESONANCE FREQUENCY VALIDATION

To verify filter stability:

$$f_{res} = \frac{1}{2\pi}\sqrt{\frac{L_c + L_g}{L_c L_g C_f}} \tag{6}$$

This frequency should be located between the grid frequency and one-half of the converter switching frequency to ensure stable control and adequate harmonic attenuation [9].

3. PASSIVE DAMPING TECHNIQUES

This chapter presents an overview of the most commonly used passive damping methods, including series damping, parallel damping, and the RC branch damping method.

3.1. SERIES DAMPING RESISTOR

In this approach, as shown in Fig 2 a resistor Rd is inserted in series with the filter capacitor Cf. This provides a direct path for resonance energy dissipation and is relatively simple to implement [11–12]. The optimal damping resistor value is typically chosen to reduce the quality factor Q of the resonant circuit. The most widely cited expressions are [11–12]:

$$R_d = \frac{1}{2\omega_{res} C_f} \tag{7}$$

$$R_d = \frac{1}{3\omega_{res} C_f} \tag{8}$$

Equation (7) is used to achieve maximum damping, while Equation (8) is preferred when aiming to reduce power loss in the resistor. The insertion of Rd flattens the resonance peak in the impedance profile and reduces the risk of instability [11–12].

The transfer function from inverter voltage to grid current for the LCL filter with series damping is:

$$G_s(s) = \frac{i_g(s)}{v_{inv}(s)} = \frac{1+R_d C_f s}{L_c L_g C_f s^3 + R_d C_f (L_c+L_g) s^2 + (L_c+L_g) s} \tag{9}$$

3.2. PARALLEL DAMPING RESISTOR

An alternative approach places Rf in parallel with the capacitor Cf as shown in Fig 2. This changes the admittance path at resonance and attenuates the oscillatory component by shunting it through the resistor [11-12]. The design of Rd is commonly based on a desired quality factor Q: The most widely cited expressions are [11–12]:

$$R_d = \frac{1}{\omega_{res} C_f Q} \tag{10}$$

Where Q is typically selected between 1.5 and 2. This method is effective in reducing resonance amplification while maintaining a simpler passive structure [11–12].

The corresponding transfer function is:

$$G_p(s) = \frac{i_g(s)}{v_{inv}(s)} = \frac{R_d}{L_c L_g C_f R_d s^3 + L_c L_g s^2 + R_d (L_c+L_g) s} \tag{11}$$

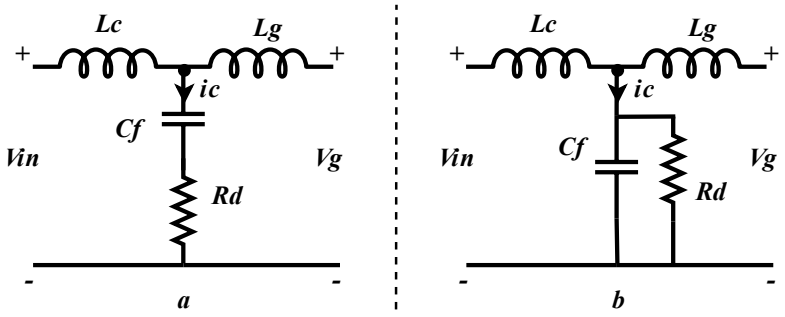

Fig. 2. Passive damping topologies for an LCL filter: (a) series damping resistor Rd in series with Cf; (b) parallel damping resistor Rd connected across Cf

3.3. R-C BRANCHE PARALLEL DAMPING RESISTOR

This method enhances frequency selectivity by connecting a resistor Rd and capacitor Cd in series and placing the branch in parallel with C_f as shown in Fig 3. It forms a notch-like damping network around the resonance frequency. The component values are determined as follows [12]:

$$R_d = \frac{1}{2\pi f_{res} C_d} \tag{12}$$

$$C_d = \frac{C_f}{n},\ n \in [5,10] \tag{13}$$

The advantage of this approach is its ability to localize damping around the resonance frequency without significantly affecting other frequency components [12].

The modified transfer function becomes:

$$G_{RC}(s) = \frac{1+R_d C_d s}{L_c L_g C_f C_d R_d s^4 + L_c L_g C_t s^3 + R_d C_d L_t s^2 + L_t s} \tag{14}$$

Where $L_t = L_c + L_g$ and $C_t = C_f + C_d$

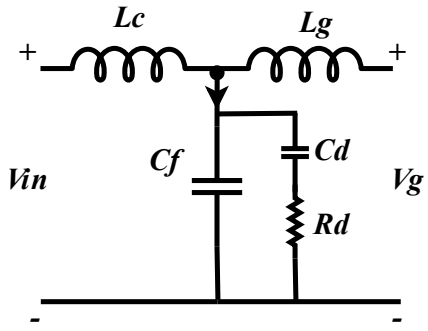

Fig. 3 RC-branch passive damping topology for an LCL filter: a series branch (R_d–Cd) connected in parallel with the filter capacitor C_f. Cd: damping capacitor; R_d: damping resistor

3.4. DESIGN CONSIDERATIONS

Among the passive damping approaches evaluated, series and parallel resistor damping offer simplicity and ease of implementation. Series Rd damping is straightforward but introduces continuous power losses and a broader frequency effect. The parallel Rd approach reduces losses and avoids increasing reactive power, making it a practical choice when compliance with grid codes is critical.

In typical LCL filter design procedures, the main filter elements– *Lg*, *Lc*, and C_f, are sized first to meet harmonic attenuation and reactive power constraints (typically ≤ 5% of rated power at 50 Hz) [8–9]. Adding C_d in parallel with C_f increases the total capacitance:

$$C_{eq} = C_f + C_d \tag{15}$$

Even a conservative selection such as Cd=Cf/10 results in approximately a 10% increase in capacitive reactive power, which may challenge grid code compliance [9]. If no headroom exists in the reactive power budget, the parallel Rd method is preferable since it avoids altering Cf. Thus, while the R–C branch offers superior damping precision, it must be applied with caution in systems tightly constrained by grid reactive power limits. Selection of the damping method should therefore balance damping strength, power loss, implementation complexity, and compliance with grid standards [11–12]. A unified comparison including active damping strategies is presented in Section 5.

4. ACTIVE DAMPING

This chapter details the implementation of capacitor-current feedback (CCF)-based active damping for a bidirectional Active Front-End (AFE) rectifier using a first-order low-pass filtered feedback path.

4.1. PRINCIPLE OF CAPACITOR-CURRENT FEEDBACK

In a typical LCL filter configuration, the resonance formed can lead to high-frequency oscillations if left undamped. Capacitor-current feedback (CCF) addresses this by introducing a virtual damping resistor across C_f. A scaled version of the capacitor current is fed back and added to the control voltage command, effectively emulating resistive damping [13–17].

4.2. MEASUREMENT AND FILTERING OF CAPACITOR CURRENT

Since bidirectional grid-connected converters typically require inverter and grid current sensing for control and protection, capacitor current estimation does not necessarily increase sensor count in practical OBC implementations. The capacitor current i_{Cf} can be measured directly or estimated by subtracting the grid-side and inverter-side inductor currents:

$$i_{Cf} = i_{inv} - i_{grid} \tag{16}$$

This three-phase current is transformed into the synchronous reference frame (d-q) using a Park transformation synchronized to the grid via a phase-locked loop (PLL). To reduce switching-frequency noise in the feedback signal, the capacitor current is passed through a first-order low-pass filter [14, 16]:

$$H(s) = \frac{1}{\tau s+1}, \tau = \frac{1}{2\pi f_c} \tag{17}$$

The cut off frequency was selected as fc = 1200 Hz, close to the LCL resonance frequency ($fres$≈1.23 kHz). This choice preserves the dominant resonance component in the capacitor-current signal while attenuating switching-frequency noise. Lower cut off frequencies would introduce additional phase lag in the damping loop, whereas higher values would allow switching harmonics to propagate through the feedback path. The resulting filter time constant is $\tau \approx 132\ \mu s$, which remains small compared with the inner current-loop dynamics.

4.3. DAMPING GAIN DESIGN

The active damping gain K_d emulates a parallel damping resistor across C_f and is designed to match the impedance at the LCL resonance frequency. It is given by [13–17]:

$$K_d = \frac{1}{\omega_{res} C_f Q} \tag{18}$$

Where: $\omega_{res} = 2\pi f_{res}$ is the resonance angular frequency, C_f is the filter capacitance, and Q is the desired quality factor (typically between 1.5 and 2).

4.4. INTEGRATION INTO AFE CONTROL STRUCTURE

The active damping signal is added after the PI controllers and before the inverse Park transformation. The total control voltage in the d-q frame is expressed as [18]:

$$v_d^* = v_d^{PI} - K_d \cdot i_{Cf,d} \tag{20}$$

$$v_q^* = v_q^{PI} - K_d \cdot i_{Cf,q} \tag{21}$$

Where: v_d^{PI}, v_q^{PI}: Outputs of the d-q current PI controllers.

$i_{Cf,d}, i_{Cf,q}$: Filtered capacitor current components in the d-q frame.

v_d^*, v_q^*: Modified voltage commands passed to the modulation stage.

This control strategy effectively emulates resistive damping at the capacitor node while maintaining fast dynamic response and stable grid-current regulation [17–18]. This sliding-mode-based approach could alternatively be implemented for higher robustness in nonlinear AFE dynamics [19].

The integration of the CCF-based active damping loop within the cascaded control structure is illustrated in Fig. 4.

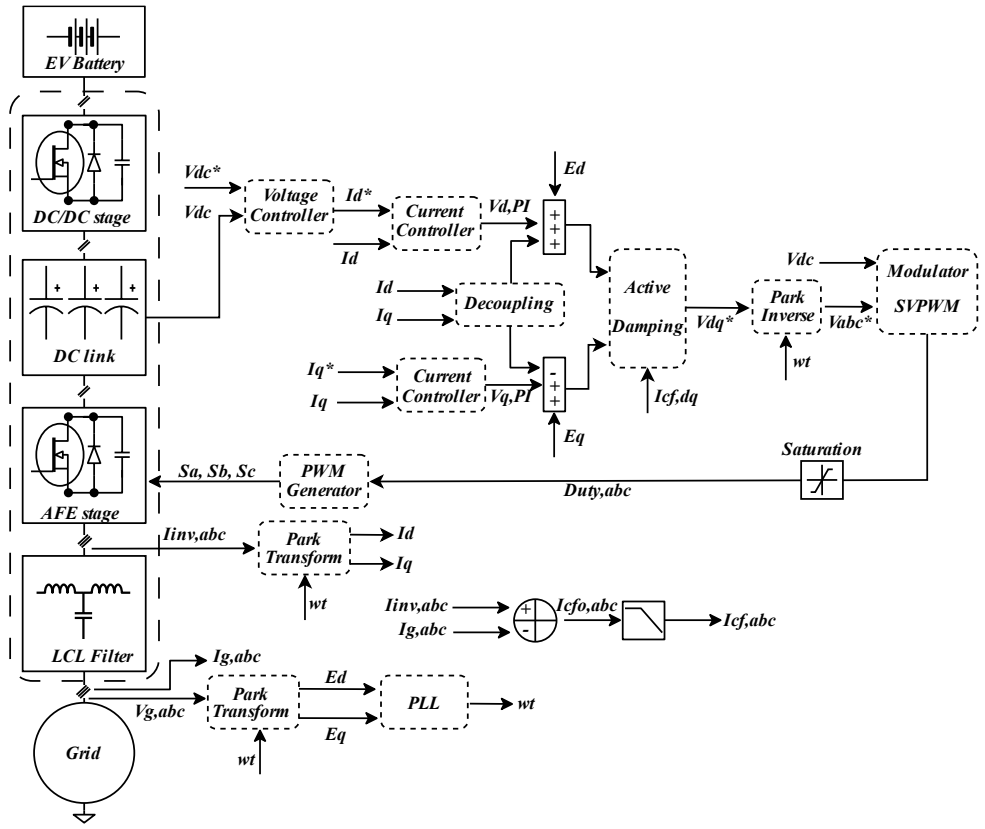

Fig. 4. Integration of capacitor-current-feedback (CCF) active damping within the cascaded AFE control structure

5. COMPARATIVE ASSESSMENT OF DAMPING STRATEGIES

Following the analytical development of passive (Section 3) and active (Section 4) damping techniques, a unified comparison is presented in Table 1 to assess their suitability for bidirectional onboard chargers (OBCs). This comparison focuses on design-level implementation aspects relevant to automotive integration, including hardware requirements, control complexity, power dissipation, reactive power impact, and robustness under bidirectional operation.

Table 1. Comparative assessment of passive and active damping strategies

Method	Added Passive Components	Added Sensors	Continuous Power Loss	Reactive Power Impact	Frequency Targeting	Bidirectional Robustness
Series Rd	+1 resistor	None	High	None	Broad	High
Parallel Rd	+1 resistor	None	Low	None	Moderate	Low-Moderate (mode-dependent)
R-C Branch	+1 resistor +1 capacitor	None	Low	Increases *Ceq*	High	High
Active (CCF)	None (Control-Based)	0–1 (depends on estimation method)	None	None	High	High

Capacitor current may be directly measured or estimated from existing inverter and grid current measurements

In practice, passive damping offers structural simplicity but introduces either resistive losses (series R_d) or reactive power modification (R–C branch). Parallel Rd reduces losses but may be sensitive under bidirectional operation. Active damping avoids passive power dissipation and preserves reactive power constraints, at the cost of increased control complexity. Therefore, damping selection in bidirectional OBC systems must balance efficiency, implementation effort, and robustness under power-flow reversal.

6. SIMULATION AND RESULTS

6.1. OVERVIEW OF THE SIMULATION SETUP

The damping strategies were evaluated using a detailed MATLAB/Simulink model of a 10-kW three-phase bidirectional onboard charger (OBC). The system (Fig. 5, Table 2) consists of an LCL-filtered Active Front-End (AFE) rectifier, an 800 V DC-link, and a bidirectional non-isolated DC/DC converter connected to a 360 V lithium-ion battery. Switches $S1$–$S6$ form the three-phase AFE bridge responsible for AC/DC conversion and DC-link regulation, while $Q1$–$Q2$ with Lo and Co implement the bidirectional DC/DC stage operating in buck mode during G2V and boost mode during V2G. A perturbation source at the grid interface is used to excite the LCL resonance during dynamic testing.

To suppress filter resonance and meet grid compliance standards, various damping techniques were implemented at the LCL interface. The AFE is controlled via a cascaded

structure comprising an outer DC-link voltage loop and inner current control loops, realized using a synchronous reference frame (dq-axis) PI controller. Space Vector PWM (SVPWM) is employed for its superior harmonic performance and DC bus utilization.

On the battery side, constant-power (CP) charging control governs energy transfer. The DC/DC stage operates in buck mode for G2V and boost mode for V2G, according to the direction of energy flow. A simulation step size of 1 μs was chosen to ensure high-resolution tracking and numerical stability.

Table 2. System Parameters

Symbol	Parameter	Value	Unit
P_r	Charger Rated Power	10	kW
V_{dc}	DC Link Voltage	800	V
C_{dc}	DC Link Capacitance	1000	μF
Q_c	Reactive power limit	≤ 5	%
ΔI	Current Ripple	≤ 20	%
V_b	Battery Nominal Voltage	360	V
—	Battery Capacity	100	Ah
f_{sw}	Switching Frequency	10	kHz
V_g	Grid Voltage (L-L)	415	V
f_g	Grid Frequency	50	Hz
L_C , L_g	LCL Filter Inductances	3.6	mH
C_f	LCL Filter Capacitance	9.24	μF

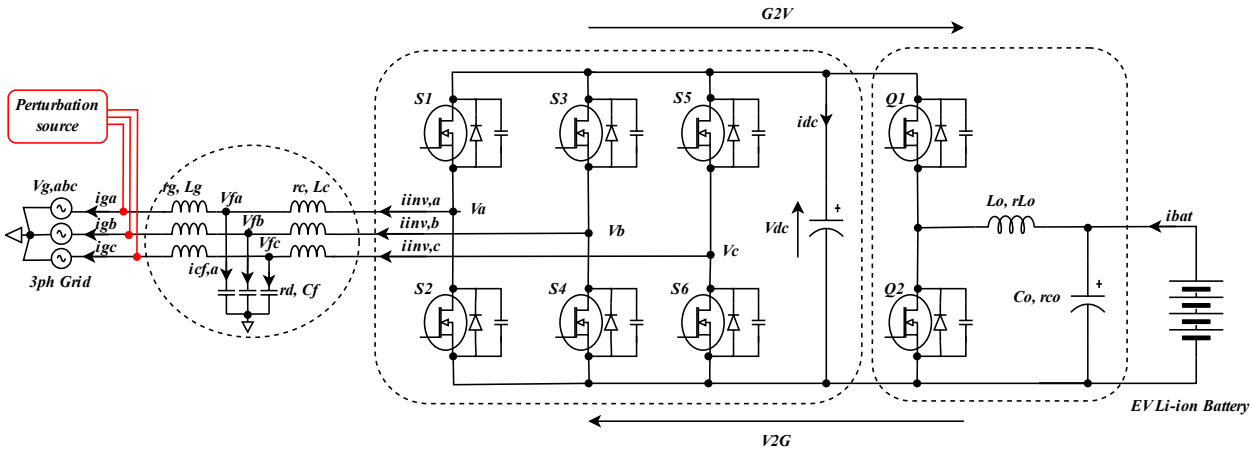

Fig. 5. Proposed bidirectional On-Board Charger (OBC) architecture used for damping evaluation

6.2. BODE PLOT VALIDATION

The first validation approach relies on frequency-domain analysis. Figure 6 presents the Bode response of the LCL filter for the undamped case and for the three passive damping configurations: series R_d, parallel R_d, and the R–C branch. In the undamped condition, a pronounced resonance peak appears near the designed frequency (~1234 Hz). The damping strategies significantly reduce this peak, illustrating their effectiveness in suppressing LCL resonance.

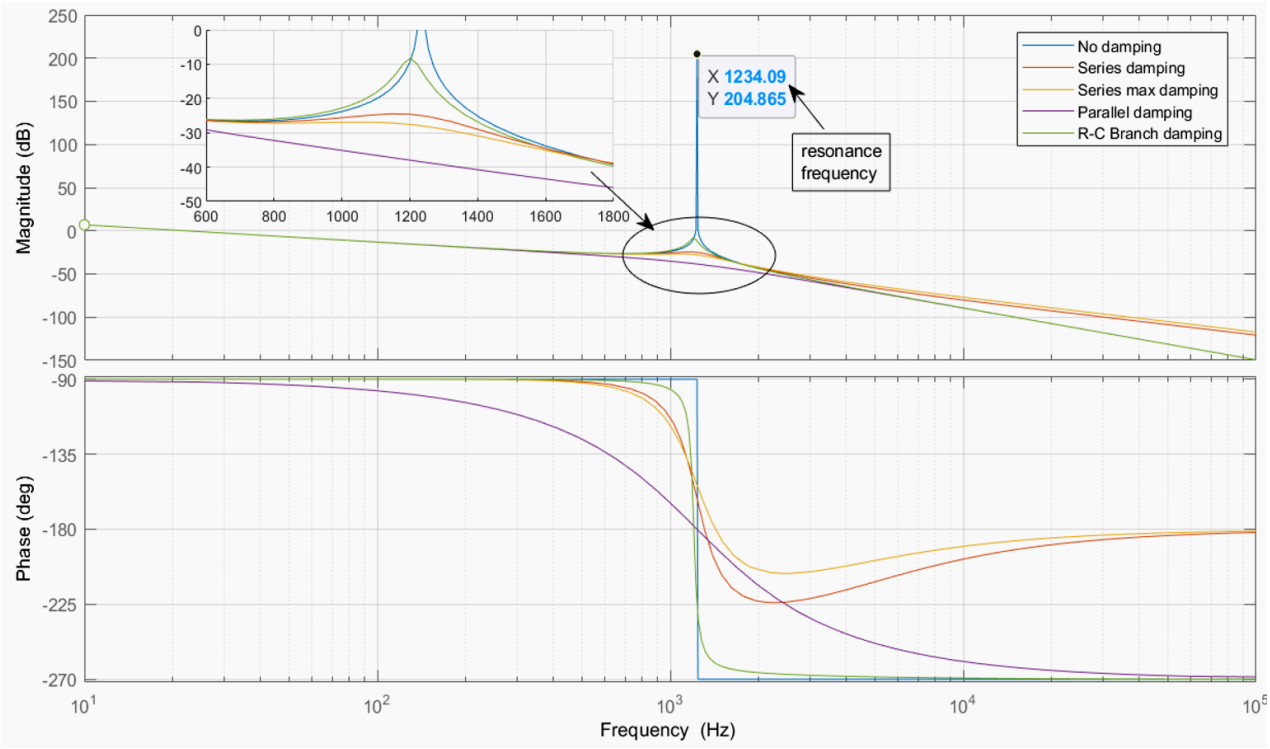

Fig. 6. Bode magnitude response comparison of the LCL filter transfer function under undamped and damped conditions (series R_d, parallel R_d, and RC-branch (R_d–C_d)). $fres$: resonance frequency

6.3. PERTURBATION-BASED EVALUATION IN SIMULINK

To evaluate damping performance under dynamic conditions, a perturbation of 20 Vrms at the resonance frequency (1234.1 Hz) was injected into the grid voltage. The perturbation was applied during 0–0.2 s in G2V mode and 0.2–0.4 s in V2G mode. The resulting grid-current response was analyzed for both passive and active damping configurations.

As illustrated in Fig. 7, the undamped case exhibits pronounced oscillations in both operating modes, confirming the inherent resonance behaviour of the LCL filter. This resonance originates from the energy exchange between the two inductors (L_c, L_g) and the filter capacitor (C_f), occurring at the characteristic frequency defined in (6). Without sufficient damping, this natural oscillatory mode can amplify grid-current disturbances and threaten closed-loop stability.

Among the passive methods, series R_d damping effectively suppresses oscillations in both G2V and V2G operation, producing stable current waveforms. Parallel R_d damping, however, exhibits asymmetric behaviour: while effective during G2V operation, it fails to maintain suppression during V2G, leading to increased distortion. The R–C branch provides balanced attenuation in both directions, although with slightly higher THD.

Active damping using capacitor-current feedback provides the most robust performance, maintaining waveform stability in both power-flow directions. Overall, the results confirm the dynamic effectiveness of the investigated methods and indicate that active damping, series R_d, and the R–C branch provide the most reliable solutions for bidirectional OBC applications.

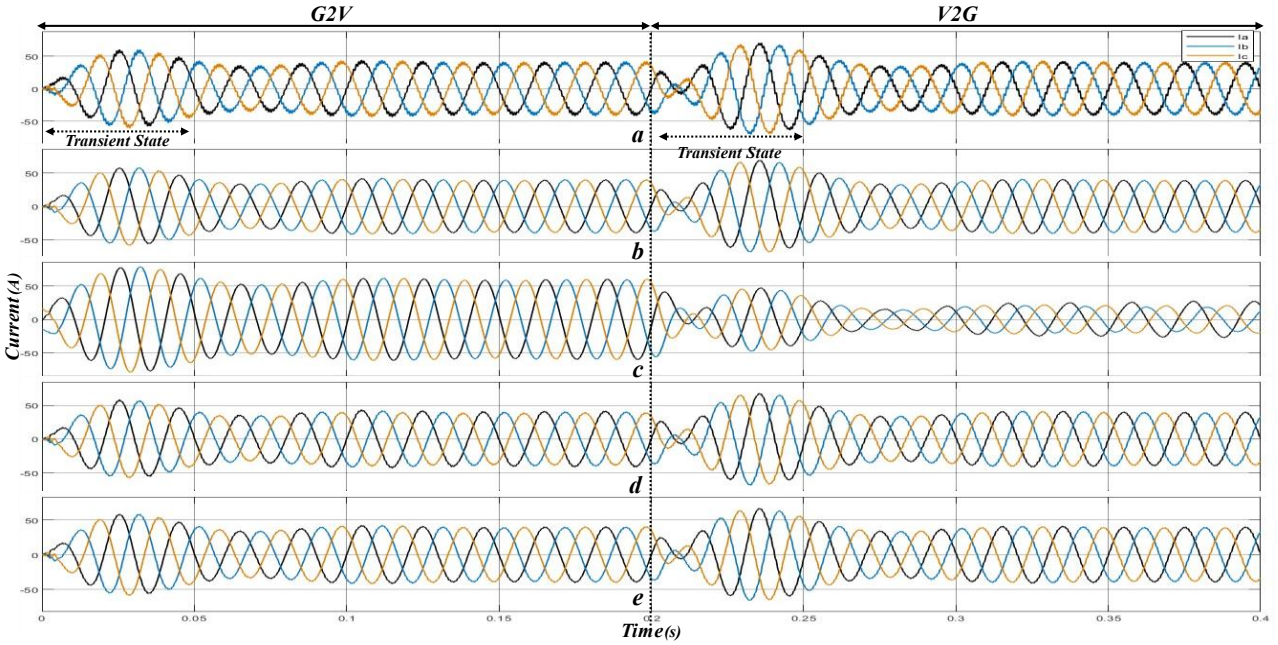

Fig. 7. Grid current response under resonance perturbation for each damping technique in both operating modes: G2V (grid-to-vehicle) and V2G (vehicle-to-grid). a) undamped LCL, b) series R_d, c) parallel R_d, d) *RC* branch (R_d–C_d)), e) active damping (CCF)

6.4. FREQUENCY-DOMAIN HARMONIC ANALYSIS, THD, AND COMPLIANCE

A MATLAB script was developed to perform the FFT analysis and extract the total harmonic distortion (THD) of the grid current for each damping method under both G2V and V2G operating modes. A representative MATLAB script and the corresponding simulation dataset used for FFT-based harmonic analysis and THD extraction are provided as supplementary material for reproducibility. Because the system is balanced, the analysis focuses on phase A, which is sufficient for harmonic evaluation. For completeness, detailed FFT spectra for the undamped case and all damping configurations are provided in the Appendix. Each spectrum includes the fundamental 50 Hz component together with the corresponding harmonic content.

The THD is computed using the standard formula:

$$THD_i = \frac{\sqrt{\sum_{n=2}^{\infty} I_n^2}}{I_1} \times 100\% \tag{22}$$

Where $I1$ denotes the fundamental current component and In represents the harmonic components.

In the undamped case, elevated harmonic levels are observed, whereas the introduction of damping techniques improves the spectral quality to varying extents, as detailed in the Appendix. Figure 8 summarizes the comparative performance metrics obtained for the different damping strategies.

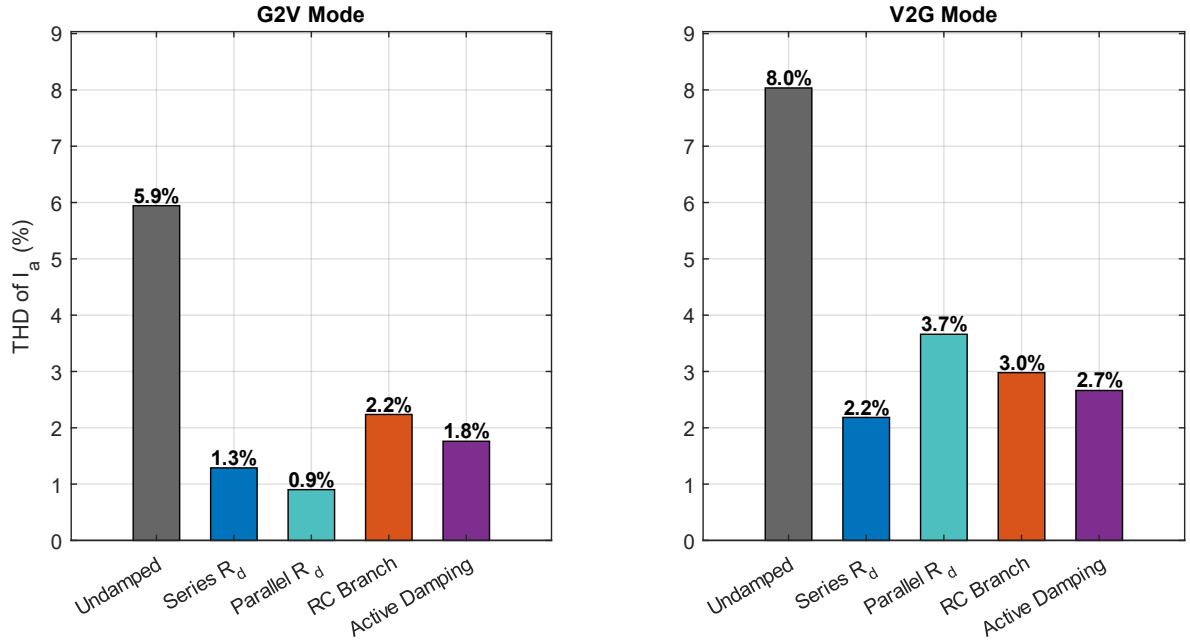

Fig. 8. Total harmonic distortion (THD) of grid current ia for each damping technique in G2V and V2G modes. THD: total harmonic distortion; G2V: grid-to-vehicle; V2G: vehicle-to-grid

6.5. COMPARATIVE SUMMARY

Damping strategies differ in both performance and implementation complexity. Series Rd damping offers a simple and robust solution, although it introduces continuous resistive losses and provides limited frequency selectivity. Active damping eliminates passive power dissipation but requires accurate current measurement and careful filter design; however, it maintains stable performance under both G2V and V2G operation without parameter reconfiguration. The R–C branch provides effective attenuation with a slight increase in reactive power, while parallel R_d damping performs well during G2V operation but exhibits poor suppression in V2G mode.

The numerical THD values reported in Table 3 are obtained from the FFT-based harmonic analysis described in Section 6.4. These results quantify steady-state grid-current distortion under both charging (G2V) and discharging (V2G) conditions, enabling a direct comparison of damping robustness under bidirectional power flow.

Table 3. Summary of THD Performance for Each Damping Technique

Technique	G2V THD (%)	V2G THD (%)	Remarks
Undamped	5.94	8.03	Resonance amplification, non-compliant THD
Series Rd	1.29	2.18	Consistent low THD in both modes, added resistive loss
Parallel Rd	0.9	3.66	Excellent G2V performance, poor V2G stability
R–C Branch	2.24	2.98	Balanced bidirectional performance, increased reactive power
Active Damping	1.76	2.66	Robust bidirectional stability without passive losses

The results suggest that damping strategy selection in bidirectional OBC systems should address not only harmonic attenuation but also stability during bidirectional operation, power loss trade-offs, and reactive power constraints.

7. CONCLUSION

This work examined passive and active damping strategies for LCL filters used in a 10-kW bidirectional onboard charger for electric vehicles. Several approaches were modelled and evaluated, including series and parallel resistive damping, *R–C* branch damping, and active damping based on capacitor-current feedback.

The simulation results demonstrate that all investigated methods attenuate the LCL resonance and reduce grid-current THD, although their effectiveness differs under bidirectional operation. Series R_d and the *R–C* branch provide stable performance in both G2V and V2G modes. In contrast, parallel Rd damping, while simple to implement, shows reduced effectiveness during V2G operation. Active damping achieves strong dynamic performance without introducing additional reactive power.

Although this study concentrates on LCL filter damping for grid stability and compliance, the complete charger architecture–including battery-side control, DC-link dynamics, and charging operation—was also modelled. A more detailed investigation of battery SOC evolution, voltage ripple, and power-regulation strategies will be addressed in future work in order to maintain the present study's focus on resonance damping and grid-side behaviour.

APPENDIX

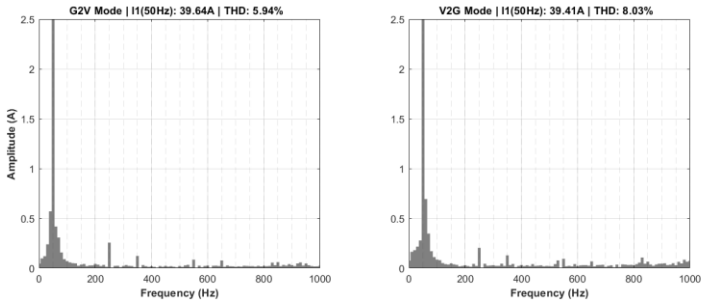

Appendix. 1. Harmonic Content of Grid Current (*Ia*) in the Undamped LCL Filter Case for G2V and V2G Modes

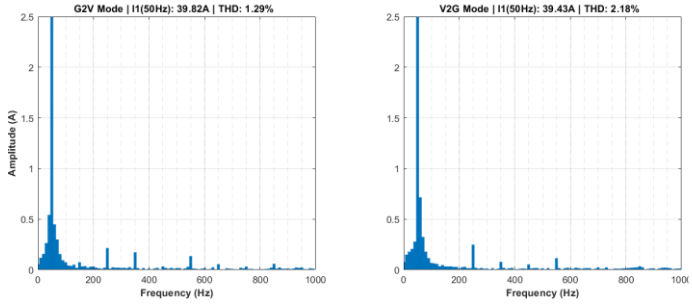

Appendix. 2. Harmonic Content of Grid Current (*Ia*) in the series damping LCL Filter Case for G2V and V2G Modes

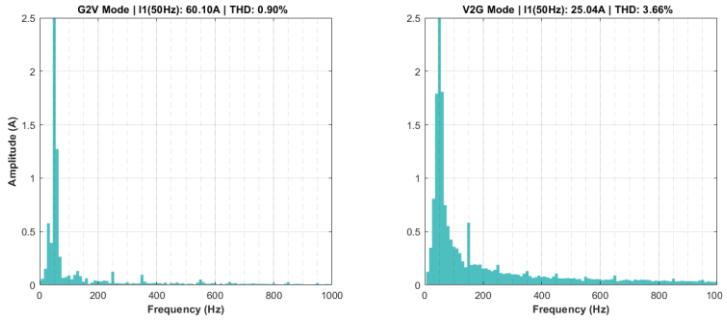

Appendix. 3. Harmonic Content of Grid Current (*Ia*) in the parallel damping LCL Filter Case for G2V and V2G Modes

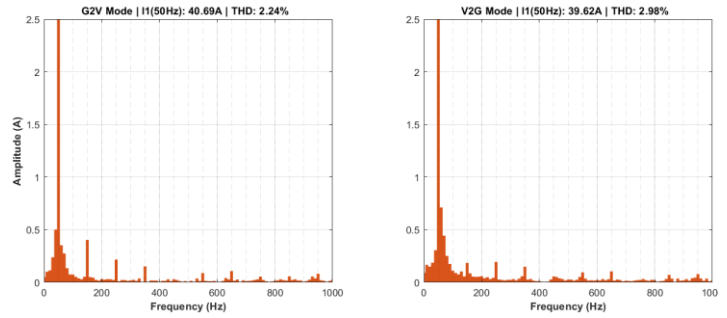

Appendix. 4. Harmonic Content of Grid Current (*Ia*) in the R-C branch parallel damping LCL Filter Case for G2V and V2G Modes

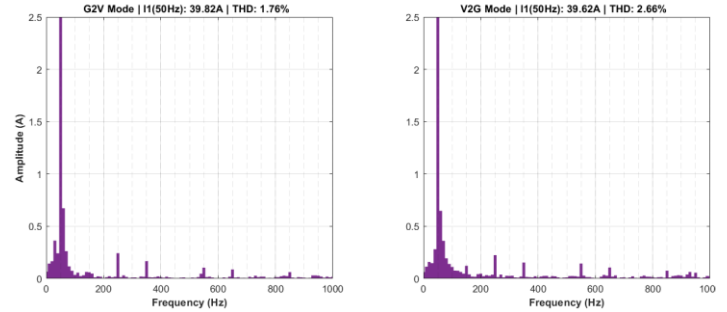

Appendix. 5. Harmonic Content of Grid Current (*Ia*) in the Active damping LCL Filter Case for G2V and V2G Modes

REFERENCES

[1] PREETHI P.J., LAL PRIYA P.S., HARI KUMAR R., 2024, *Design and Control of Bidirectional Onboard Charger for an Electric Vehicle*, Advanced Technologies in Electric Vehicles, 483–504, https://doi.org/10.1016/b978-0-443-18999-9.00022-3.

[2] VEERAKGOUNDAR V., SUBRAMANIAM S., 2025, *An Efficient and Compact Voltage Feed-Forward DAB-Based Bidirectional DC–DC Converter for Onboard EV Charger*, Computers and Electrical Engineering, 122, 109979, https://doi.org/10.1016/j.compeleceng.2024.109979.

[3] DIOURI A., KHAFALLAH M., HASSOUNE A., MESKINI M.A., 2023, *Bi-Directional Battery Charging/Discharging Converter for Grid Integration: A Step Towards Power Quality and Efficient Energy Management in Electric Vehicles*, E3S Web of Conferences, 469, 00053, https://doi.org/10.1051/e3sconf/202346900053.

[4] DIOURI A., KHAFALLAH M., HASSOUNE A., MESKINI M.A., 2025, *An Integrated Energy Management Strategy for Efficient Power Flow in EV on-Board Chargers with V2G Capability*, EPJ Web of Conferences, 330, 07001, https://doi.org/10.1051/epjconf/202533007001.

[5] KUMAR P., et al., 2025, *A Comprehensive Review of Vehicle-to-Grid Integration in Electric Vehicles: Powering the Future*, Energy Conversion and Management: X, 25,100864, https://doi.org/10.1016/j.ecmx.2024.100864.
[6] ALI M.I., MANDAL R., KUMAR A., 2024, *High-Performance Single-Phase Bi-Directional Novel on-Board Charger for Electric Vehicles*, Energy Storage, 6/5, https://doi.org/10.1002/est2.70014.
[7] SAXENA S., FARAG H., NASR K., ST. HILAIRE L., 2023, *Field Testing of Residential Bidirectional Electric Vehicle Charger for Power System Applications*, 12th International Conference on Renewable Energy Research and Applications (ICRERA), 62–66, https://doi.org/10.1109/icrera59003.2023.10269412.
[8] SAID-ROMDHANE M.B., NAOUAR M.W., SLAMA BELKHODJA I., MONMASSON E., 2016, *Simple and Systematic LCL Filter Design for Three-Phase Grid-Connected Power Converters*, Mathematics and Computers in Simulation, 130, 181–193, https://doi.org/10.1016/j.matcom.2015.09.011.
[9] XU J., XIE S., 2017, *LCL-Resonance Damping Strategies for Grid-Connected Inverters with LCL Filters: A Comprehensive Review*, Journal of Modern Power Systems and Clean Energy, 6/2, 292–305, https://doi.org/10.1007/s40565-017-0319-7.
[10] KE S., LIANG B., 2024, *A Joint Active Damping Strategy Based on LCL-Type Grid-Connected Inverters for Grid Current Feedback and PCC Voltage Unit Feedforward*, Sensors, 24/18, 6029, https://doi.org/10.3390/s24186029.
[11] TANG X., ZHANG D., CHAI H., 2021, *Synthetical Optimal Design for Passive-Damped LCL Filters in Islanded AC Microgrid*, Journal of Energy and Power Technology, 03/03, https://doi.org/10.21926/jept.2103032.
[12] CHTOUKI I., ZAZI M., FEDDI M., RAYYAM M., 2016, *LCL Filter with Passive Damping for PV System Connected to the Network*, International Renewable and Sustainable Energy Conference (IRSEC), 692–697, https://doi.org/10.1109/irsec.2016.7984020.
[13] ZHANG X., XIE Y., WU R., 2024, *A Capacitor-Current-Feedback Active Damping Control Strategy with Phase Lead Compensation for LCL-Type Grid-Connected Inverter*, IEEE Access, 12, 193663–193675, https://doi.org/10.1109/access.2024.3497004.
[14] CHEN W., ZHANG Y., TU Y., GUAN Y., SHEN K., LIU J., 2023, *Unified Active Damping Strategy Based on Generalized Virtual Impedance in LCL-Type Grid-Connected Inverter*, IEEE Transactions on Industrial Electronics, 70/8, 8129–8139, https://doi.org/10.1109/tie.2022.3232647.
[15] LISERRE M., BLAABJERG F., HANSEN S., 2005, *Design and Control of an LCL-Filter-Based Three-Phase Active Rectifier*, IEEE Transactions on Industry Applications, 41/5, 1281–1291, https://doi.org/10.1109/tia.2005.853373.
[16] DANNEHL J., WESSELS C., FUCHS F.W., 2009, *Limitations of Voltage-Oriented PI Current Control of Grid-Connected PWM Rectifiers with LCL Filters*, IEEE Transactions on Industrial Electronics, 56/2, 380–388, https://doi.org/10.1109/tie.2008.2008774.
[17] LORZADEH I., ASKARIAN ABYANEH H., SAVAGHEBI M., BAKHSHAI A., GUERRERO J., 2016, *Capacitor Current Feedback-Based Active Resonance Damping Strategies for Digitally-Controlled Inductive-Capacitive-Inductive-Filtered Grid-Connected Inverters*, Energies, 9/8, https://doi.org/10.3390/en9080642.
[18] BAO C., RUAN X., WANG X., LI W., PAN D., WENG K., 2014, *Step-By-Step Controller Design for LCL-Type Grid-Connected Inverter with Capacitor–Current-Feedback Active-Damping*, IEEE Transactions on Power Electronics, 29/3, https://doi.org/10.1109/tpel.2013.2262378.
[19] TRAN Q.-T., 2024, *Control of a Grid-Connected Inverter Using Sliding Mode Control*, Engineering, Technology & Applied Science Research, 14/3, 14558–14565, https://doi.org/10.48084/etasr.7335.